Desalination 582 (2024) 117511

Contents lists available at ScienceDirect

Desalination

journal homepage: www.elsevier.com/locate/desal

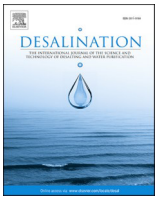

Productivity, selectivity, and energy consumption of pilot-scale vacuum assisted air-gap membrane distillation for the desalination of high-salinity streams

Marco Malaguti [a], Luke K. Presson [b,c], Alberto Tiraferri [a], Kerri L. Hickenbottom [b,c], Andrea Achilli [b,c,*]

[a] Department of Environment, Land and Infrastructure Engineering, Politecnico di Torino, C.so Duca degli Abruzzi 24, 10129 Torino, Italy
[b] Department of Chemical and Environmental Engineering, University of Arizona, Tucson, AZ 85721, United States
[c] Water and Energy Sustainable Technology (WEST) Center, University of Arizona, Tucson, AZ 85745, United States

HIGHLIGHTS

- Productivity, selectivity, and energy consumption were investigated in AGMD.
- Feed flow rate and applied vacuum solidly correlate with distillate flux and STEC.
- The distillate quality is regulated by the relative rate of vapor and liquid flow.
- The total pressure difference across the membrane governs the system rejection.

GRAPHICAL ABSTRACT

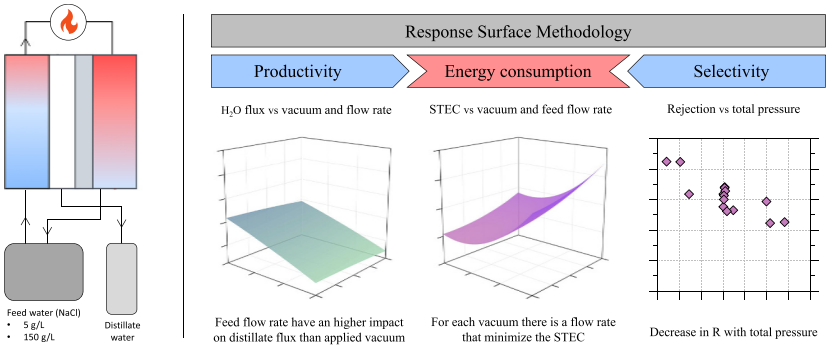

ARTICLE INFO

Keywords:
Air gap membrane distillation
Pilot-scale
Performance
Hyper-saline streams
Pore flow

ABSTRACT

The implementation of air gap membrane distillation systems is limited by a lack of overall performance predictions which rely on few available pilot-scale studies. This study evaluates the productivity, energy consumption, and selectivity of a pilot-scale air gap membrane distillation system by combining experiments and modeling activities. The effect of operating conditions, i.e., applied vacuum, feed flow rate, and feed stream salinity, was investigated to identify regulating factors and quantify dependencies. Response surface methodology was applied to model the phenomena and provide statistical analysis. Increasing flow rates produced a near linear increase of productivity within the investigated range. Operating at higher applied vacuum also translated into enhanced productivity, though the distillate flux increased by a maximum of 10 % when vacuum increased from −100 mbar to −500 mbar. Flow rate and vacuum also governed the observed salt flux by a similar magnitude because salt flux resulted mainly from liquid pore flow phenomena. The trans-membrane pressure regulated the membrane rejection: increasing the pressure difference led to a lower rejection. Moreover, high feed stream salinity lowered both the productivity and the distillate quality. The productivity gains were typically achieved at the expense of an increase in specific thermal energy consumption; however, an interesting

* Corresponding author at: Department of Chemical and Environmental Engineering, University of Arizona, Tucson, AZ 85721, United States.
E-mail address: achilli@arizona.edu (A. Achilli).

https://doi.org/10.1016/j.desal.2024.117511
Received 23 November 2023; Received in revised form 6 March 2024; Accepted 6 March 2024
Available online 21 March 2024

relation was observed with feed stream salinity, with a minimum of specific thermal energy consumption of roughly 300 $kWh_{th}·m^{-3}$ identified in the treatment of a stream with a salinity of 150 g/L.

1. Introduction

The increasing demand for safe freshwater, together with efforts to reduce the impacts of brine management, are leading to the growth of zero liquid discharge (ZLD) strategies and technological solutions [1,2]. Membrane-based separation processes participate toward achieving ZLD in agricultural, industrial, and desalination applications [3–6]. In particular, membrane distillation (MD) is gaining interest from both the scientific community and industrial stakeholders, because it can desalinate high-salinity streams up to substantial water recovery rates [7–10]. MD is a thermally-driven process that exploits a temperature difference between the two sides of a porous hydrophobic membrane to create a vapor pressure difference, which leads to the transport of vapor across the membrane pores. Despite its high energy consumption, MD has higher degree of flexibility in terms of feed salinity in comparison to reverse osmosis desalination and it can be powered with low-grade heat and renewable energy sources [11–13].

Although a significant amount of research on MD has been carried out in the last decades, full-scale MD systems have not yet reached commercial feasibility, partly because pilot-scale investigations aimed at scaling-up the technology are limited by the complexity of scale-up operations [14]. Technical and economic assessments of MD cannot be accurately performed with the results of bench-scale studies because of differences in scale and testing procedures [15,16]. Pilot-scale research is critical to retrieve accurate description of performance and to infer adequate predictions of the behavior of MD systems at full-scale [17,18].

Among the possible MD configurations, vacuum-assisted air gap membrane distillation (V-AGMD) utilizing spiral-wound modules is advantageous in terms of water production and energy efficiency compared to others [19,20]. The concept underlying V-AGMD configuration is the increase of distillate water production achievable by exploiting the removal of air (creation of a vacuum) from the gap of the module. The vacuum decreases the vapor pressure in the air gap and membrane pores, which consequently decreaes the mass resistance to distillate production [21]. This conceptualization was applied in an early stage bench-scale version by Winter et al. in 2011 [22], and subsequently scaled up and commercialized in different configurations by the company Aquastill. Moreover, a comprehensive evaluation of the V-AGMD systems should also take into account the process energy consumption and the quality of the product water. Several energy analyses have been performed to identify the most efficient configurations, sizes, and sources of exergy losses in AGMD systems [13,23,24]. However, both feed stream salinity and operating conditions substantially influence the absolute energy needs and the relative contribution of different energy sources. For what concerns the distillate quality, it has been shown that increasing the feed salinity typically worsens the quality of the product water [17,25]. In terms of operating conditions, Ruiz-Aguirre et al. suggested that the distillate quality may not depend on the operating conditions under ideal scenarios, and that the electrical conductivity differences in the product water that are commonly recorded in experimental investigations might be mainly due to membrane surface defects [14,26].

In this study, a multi-parameter investigation is presented with the goal of narrowing the gap in the understanding of V-AGMD systems behavior and scalability. Specifically, the performance of a pilot-scale V-AGMD system is discussed considering the productivity of the process, the energy consumption, and the product water quality. Response surface methodology (RSM) was applied to model the performance of the investigated MD system [6,27–29]. The control variables of the model, i.e., the operating parameters investigated in the experimental campaign, were the feed flow rate, the applied vacuum, and the feed stream salinity (NaCl concentration). The analyzed responses of the model, i.e., the experimental outcomes retrieved with statistical significance by the tuned model, were the distillate flux, the temperature difference between the condenser outlet and the evaporator inlet, and the associated specific thermal energy consumption (STEC). In addition, the specific electrical energy consumption (SEEC) was evaluated to provide a comprehensive view of the energy requirements. Due to the limitations of using the absolute distillate quality in correctly describing the system selectivity, both membrane rejection and salt flux were evaluated to achieve a more mechanistic and less system-specific discussion. To conclude, the normalized solute flux with respect to feed stream salinity was analyzed to give insights on selectivity in terms of membrane wetting and membrane surface defects.

2. Materials and methods

2.1. Description of the unit

The experimental campaign was performed using a pilot-scale V-AGMD system (Aquastill, Sittard, the Netherlands) that was operated at the Water and Energy Sustainable Technology (WEST) Center (Tucson, AZ). A schematic of the unit is reported in Fig. 1. The pilot-scale system is composed of a feed stream circulation loop and separated heating and cooling loops with heat exchangers used to regulate the feed water temperature at the inlet of both the cold side ($T_{cold,in}$) and the hot side ($T_{hot,in}$).

Through a centrifugal pump (Arbo pumps, Smilde, the Netherlands) connected to the feed reservoir, the feed solution first passed through the heat exchanger of the cooling loop to lower its temperature until the set-point was reached in each of the tests (blue line). The cooling loop operated with a constant flow of service water available onsite. The cooling loop was equipped with a narrowing section, connected to the distillate reservoir (green dashed line), to generate vacuum by the Venturi effect. The vacuum was deployed in the distillate line to promote vapor flow through the membrane pores and its desired level was regulated through an adjustable relief valve that ensured a setting precision always higher than 95 %. After cooling, the feed stream entered the membrane cold channels to serve as a gap cooling stream. The stream gained heat by conduction from the other membrane side together with latent heat from the vapor re-condensing in the gap and was thus preheated as it exited the cold channel. Its temperature was further increased passing through the heat exchanger of the heating loop until the set-point was reached and the feed stream entered the hot channels (red line). The heating loop comprised of a submersed coil hosting a flow of service water heated by an electrical resistance. The difference in vapor pressure due to the temperature gradient between the two sides of the membrane drove the vapor from the hot channel through the membrane pores to the air-gap where it condensed on the condensing plate. The produced distillate was collected in the distillate tank until reaching a volume of 3.5 L and was automatically recirculated into the feed reservoir. After the feed stream exited the hot channels of the module it diretly re-entered the feed reservoir. In this closed loop configuration, the feed stream concentration was held constant to perform experiments at a fixed salinity value. The V-AGMD unit was equipped with hydraulic pressure sensors at both the feed hot and cold inlets while temperature sensors were present at the cold inlet, cold outlet, hot inlet, and hot outlet of the feed loop, as well as at the outlet of the distillate channel. All of the sensors were monitored by a digital interface and the values recorded by a programmable logic controller (PLC) every 10 s. For this research a new membrane was utilized. The membrane characteristics provided by the manufacturer are reported in

Table 1 together with further information reported in Fig.S1 and Table S1 in the Supporting Information. The salt rejection measured by the manufacturer was obtained with tap water as feed stream, operating at feed temperatures of 80 °C – 20 °C.

2.2. V-AGMD performance estimators

The performance of the V-AGMD system was evaluated in terms of productivity, specific thermal energy consumption, specific electrical energy consumption, salt rejection, and salt flux. All experiments were performed at constant $T_{hot,in}$ and $T_{cold,in}$ equal to 70 °C and 30 °C, respectively. Data were automatically recorded every 10 s in steady-state conditions to prove the reliability of the performance in long-term operations. To ensure that the steady-state was reached, each experiment was performed for a duration of at least 6 h [30]. All of the experiments were performed recirculating continuously the distillate water into the feed tank. Therefore, the overall system recovery could be assumed to be approximately 0 % (no considerable amount of water lost during the experiment) while the single pass water recovery of the module (fraction of distillate water produced by the module in a unit time with respect to the influent flow rate) that can be directly calculated as $J_w \cdot A \cdot Q_f^{-1}$ was always lower than 4 %.

The productivity of the unit was assessed by computing J_w, the distillate flux across the membrane, as given in Eq. (1).

$$J_w = \frac{V_d}{A \cdot \Delta t} \tag{1}$$

where A is the active area of the membrane and V_d is the volume of distillate water collected in the time frame Δt. Both the thermal and the electrical energy consumption were assessed. The thermal analysis was performed analyzing the STEC, which is widely used since it expresses the external thermal energy input necessary to produce one cubic meter of distillate water. The STEC was computed according to Eq. (2).

Table 1
AGMD module and membrane characteristics.

Parameter	Unit	Value
Membrane material	–	Polyethylene
Number of channels	–	12
Membrane active area	m^2	25.92
Channel length	m	2.7
Nominal pore size	μm	0.3
Thickness	μm	96
Porosity	%	85
Liquid entry pressure	bar	4.2
Manufacturer measured salt rejection	%	99.75

$$STEC = \frac{Q_f \cdot \rho_f \cdot C \cdot \left(T_{hot,in} - T_{cold,out}\right)}{J_w \cdot A \cdot 3.6 \cdot 10^6} \tag{2}$$

where Q_f is the feed flow rate, ρ_f is the feed density, and C is the specific heat capacity that is assumed to be constant. The SEEC indicates instead the electrical energy consumed per volume unit of distillate product and was calculated using Eq. (3). Only the electrical energy needed to circulate the water trough the membrane channels was evaluated, while the energy consumption related to the vacuum generation and to the cooling of the feed stream were not considered due to the configuration of this specific system (Venturi effect for vacuum and service water stream for cooling).

$$SEEC = \frac{Q_f \cdot \Delta P_{drop}}{36 \cdot \eta \cdot J_w \cdot A} \tag{3}$$

where η is the efficiency of the water-circulating pump, assumed equal to 70 % to obtain a conservative estimation, while ΔP_{drop} is the hydraulic pressure drop over the entire membrane module, i.e. $P_{cold,in} - P_{hot,out}$ in

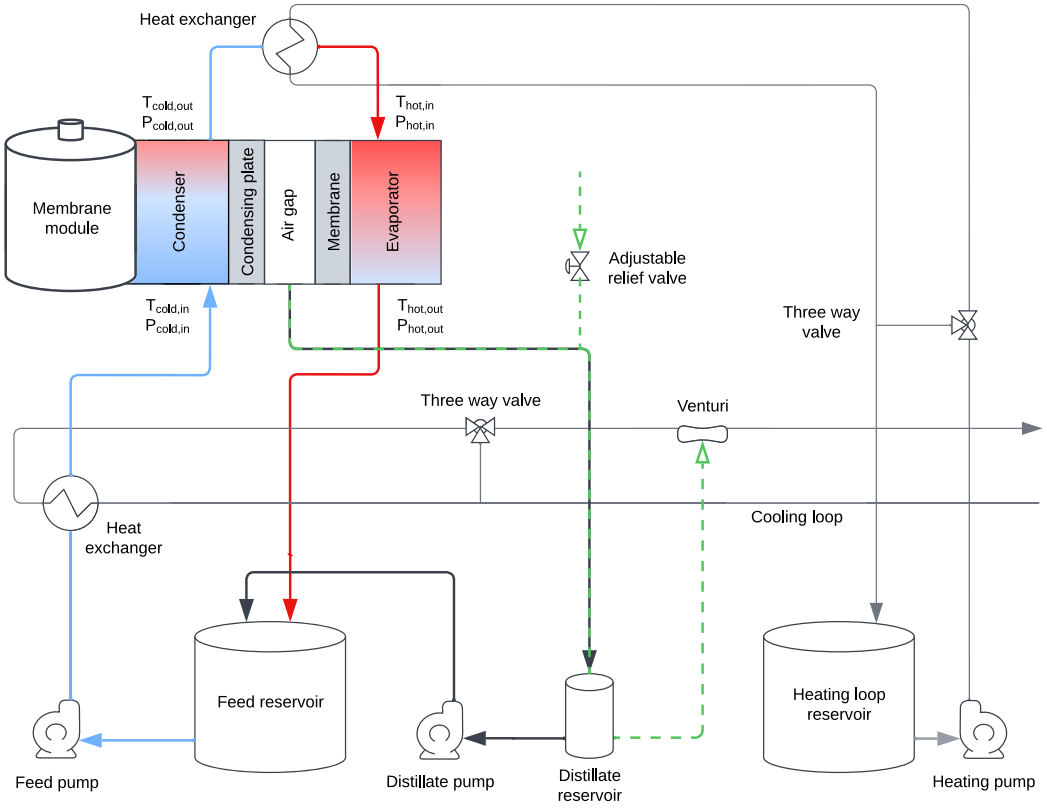

Fig. 1. Schematic representation of the pilot-scale V-AGMD system used to perform the experiments. Blue lines represent cold/chilled streams, red lines refer to hot streams, bold black lines refer to the distillate product, green dashed lines refer to air/vacuum, while normal black lines refer to service water streams.

reference to Fig. 1. As the outlet of the evaporator channel is open to the atmosphere, it can be assumed that its relative pressure is close to zero and thus ΔP_{drop} was calculated directly as the feed cold inlet pressure level, assuming the value of the feed hot outlet negligible to give a conservative estimation.

To assess the selectivity of the process, the salt passing through the hydrophobic membrane was attributed to the pore flow phenomenon: water flows through membrane pores in the liquid phase, consequently transporting the dissolved species. In the presence of pore flow, the total distillate flux is the sum of the vapor flux and the liquid flux as reported in Eq. (4).

$$J_w = J_{w,v} + J_{w,l} \tag{4}$$

In the absence of membrane scaling and other chemical wetting agents, pore wetting is mainly caused by operating at trans-membrane pressure (TMP) that exceeds the membrane liquid entry pressure (LEP) of a fraction of the pores. Since membranes present a distribution of pore size, larger diameter pores inevitably contribute to pore flow even at low pressure levels [931–33]. Note that in V-AGMD the TMP is calculated as the sum of the evaporator channel pressure (average value along the module) and the value of the vacuum. Consequently, the transport of non-volatile solutes across the membrane due to pore flow, i.e., the salt flux, J_s, can be evaluated as a function of either the liquid distillate flux or the total distillate flux, as given in Eq. (5).

$$J_s = J_{w,l} \cdot c_f = J_w \cdot c_d \tag{5}$$

where c_f and c_d are the concentrations of NaCl in the feed stream and in the produced distillate water, respectively. In strict terms, c_f in Eq. (5) should be considered as the average concentration of the salty feed stream inside the evaporator channel, and not simply as the inlet bulk feed concentration. However, as the single pass recovery rate of the module was small, typically between 1 % and 3 % for the various tests and always <4%, the difference between these two concentrations may be considered negligible in this study. Note that these equations are specific to V-AGMD systems and may not be applicable to other MD configurations. It is worth highlighting that the solution electric conductivity was measured instead of the salt concentration, as the former can be used as proxy for the latter within concentration ranges whereby the two parameters have a linear relationship. As extensively discussed in previous literature studies, this relationship may be confidently assumed to be linear at values of salt concentration lower than approximately 150 g/L as shown by the correlation reported in Fig.S2 in the Supporting Information [14]. The last parameters used to evaluate the selectivity of the process were the salt rejection, R, and the log removal value, LRV, calculated according to Eq. (6) and Eq. (7) respectively.

$$R = \left(1 - \frac{c_d}{c_f}\right) \cdot 100 \tag{6}$$

$$LRV = log_{10}\left(\frac{c_f}{c_d}\right) = -log_{10}\left(1 - \frac{R}{100}\right) \tag{7}$$

Note that LRV directly correlates to rejection: 90 % rejection translates to a LRV of 1 while 99 % rejection translates to a LRV of 2. c_f is the electric conductivity measured in the feed tank, which may be considered constant because the experiments were performed under near steady-state conditions with both the concentrate and the distillate streams being recirculated into the feed tank. On the other hand, c_d is the average electric conductivity value measured in the distillate pipe exiting the module throughout the test. The distillate stream electric conductivity was practically constant (low standard deviation) during each test, owing to steady-state conditions. Once again, note that c_f represents the inlet bulk feed conductivity, not the average bulk conductivity of the salty stream in the evaporator channel, the latter increasing along the module as water recovery increased, while c_d represents the conductivity from the distillate flow coming from the entire module. Therefore, rejection calculated with Eq. (6) should be rigorously regarded as an observed "module rejection" rather than an observed "membrane rejection", which would require associating c_d with the average bulk conductivity of the salty stream within the module. That being said, since as aforementioned the recovery rate of the module was small, the change in c_f or c_d along the module may be considered negligible and the results obtained by applying Eq. (6) may be interpreted in this study as "membrane rejection" values for all practical purposes.

2.3. Design of experiments, statistical analyses, and experimental procedures

The software Design Expert was used to design the experimental campaign based on RSM through the application of central composite design (CCD), which defined the number of experiments and the values of the variables needed for the statistically significant assessment of the variables and responses. In addition, to understand the process behavior under high salinity conditions, represented by a feed stream NaCl concentration of 150 g/L, experiments were also conducted at low salinities of 1 g/L and 5 g/L representing control scenarios and allowing easier highlight of the effect of salinity. The statistical ranges of variable values are reported Table 2, together with the experimental ranges necessary to properly build the response surface through CCD and to probe the entire multidimensional space. In this scenario, 13 experiments were performed for each salinity, 8 of them at different values of flow rate and vacuum, together with 5 replicates of the central point. The collected experimental results were used as input data to generate the model for each response according to the best quadratic fit. Analysis of variance (ANOVA) was used to analyze the statistics and to evaluate the quality of the obtained model.

3. Results and discussion

3.1. Relationship between applied vacuum, feed flow rate, and productivity

The steady-state distillate fluxes observed in the experiments are reported against feed flow rate and applied vacuum in Fig. 2. An increase in feed flow rate always translated into higher distillate fluxes, i.e. productivity, regardless of the vacuum value. This trend was described also in a research report by Eykens et al. [34] and in a review by Chen et al. [33]. Also an increase in applied vacuum led to greater productivity, while the impact of this second operating variable was substantially lower than that of feed flow rate. These trends are well exemplified by comparing the results of the various experiments performed at −100 mbar with those obtained at −500 mbar vacuum, under the same feed flow rate values. While doubling the feed flow rates translated into a similar increase in distillate flux, operating at a vacuum five times higher only resulted in slightly larger productivity, up to approximately 10 % of gain; see Fig. 2, second and fourth panel. In a previous research, Liu et al. [35] suggested that even if an increase in vacuum inside the air gap lowered the resistance in the pores while enhancing the vapor pressure difference and therefore the driving force, the recorded productivity improvements were barely more than 10 %. The data plotted in Fig. 2 also imply that feed stream salinity is an important factor regulating productivity because the distillate flux in the hyper-saline

Table 2
Experimental design of the selected operating conditions, representing the range of variable values of the RSM model.

Controls	Unit	Modeling range	Experimental range
Vacuum	mbar	100–500	17–583
Feed flow rate	$L{\cdot}h^{-1}$	600–1,200	476–1,324

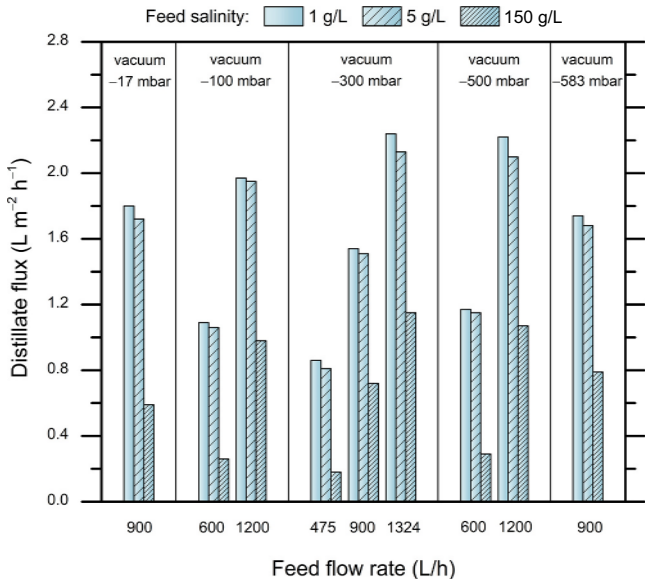

Fig. 2. Steady-state distillate flux (y-axis) is reported as a function of feed flow rate (x-axis) and applied vacuum (panels). The solid bars refer to a feed stream containing 1 g/L of NaCl, the sparsely patterned bars refer to a feed stream containing 5 g/L of NaCl, while the densely patterned bars are related to a concentration of 150 g/L. This data is used to build the respond surface for the distillate flux. For the central point, i.e. Q_f equal to 900 L/h and applied vacuum equal to −300 mbar, the five replicates showed negligibly different results, i.e., within 2 %, and for this reason standard deviation bars cannot be observed.

scenario (150 g/L) was substantially lower than that observed in the low salinity cases (1 g/L, 5 g/L). For this reason, and due to the strong similarity between the results obtained at 1 g/L and 5 g/L, the following sections will only discuss results related to 5 g/L and 150 g/L feed stream salinities. In summary, the observed productivity were coherent with available literature studies performed with similar configurations, modules size, as well as evaporator and condenser temperatures [15,19,25,27,31,36]. Specifically, distillate fluxes between 0.5 LMH and 2.5 LMH were observed for low to medium salinity scenarios while distillate fluxes lower than 1.5 LMH were typically measured when using hyper-saline feed streams. Based on the distillate flux results discussed just above, the response surfaces were built for the 5 g/L scenario (Fig. 3a) and for the 150 g/L scenario (Fig. 3b). Details regarding the set of results used to develop the model (Tab.SA1 and Tab.SA3) together with the outcome of the statistical analysis (Tab.SA2 and Fig.SA1, Tab. SA4 and Fig.SA2) are reported in the appendix of the Supporting Information. The graphs in Fig. 3 report the surface of the distillate flux values modeled as a function of feed flow rate and applied vacuum. Despite absolute values being substantially higher for the low salinity feed, the two surfaces present analogous shape that supports the reliability of the results and confirms that the impact of feed flow rate was dominant compared to that of applied vacuum. This may be due to the reduced temperature drop occurring along the module at high feed flow rates, i.e., better preservation of the bulk temperature and thus of the driving force. In addition, another beneficial effect of increasing the feed flow rate is the consequent reduction of both temperature and concentration polarization due to increased channel heat and mass transfer coefficients [36]. On the other hand, the loss in productivity due to salinity accounts for a decrease of around 50 % between the two cases, as similarly shown in a previous research [25]. Moreover, it is worth mentioning that the quadratic surface in Fig. 3a shows a minimum distillate flux at mid vacuum values. This might be suggesting that the decrease in temperature difference when increasing the applied vacuum (as observed in Fig. 4a and discussed in the next paragraph) generates a decrease in driving force that is more significant than the lowered resistance in the pores due to vacuum increase itself, until around −300 mbar when the latter effect becomes dominant. On the other hand, the minimum in the distillate flux shown in Fig. 3a may be due to the mathematical nature of the quadratic function deployed to fit the surface response, and it might not be due to a physical phenomenon. However, note that using a linear or a quadratic response surface results in minor differences, considerable smaller than the experimental uncertainty of the data. However, these pilot-scale results and their absolute values of distillate flux suggest that in a real scale operation an increase in productivity would be more easily pursued by selecting a larger feed flow rate instead of enhancing the applied vacuum. In addition, it is worth noting that both surfaces present a pseudo-linear behavior. This observation implies that the performance improvement obtained by increasing the operating parameters may be considered largely independent of the initial conditions.

3.2. *Relationship between applied vacuum, feed flow rate, and energy consumption*

In general, according to the definition of STEC reported in Eq. (2), an increase in distillate flux, a decrease in feed flow rate, and/or a decrease in temperature difference between the cold outlet and the hot inlet, translate into a lower specific thermal energy consumption. The energy performance of the process lays on the trade-off behavior of these various parameters and their relative impacts. To address these phenomena, the response surfaces were firstly built for the temperature difference between the evaporator inlet and the condenser outlet. This temperature difference influences the STEC since the latter is

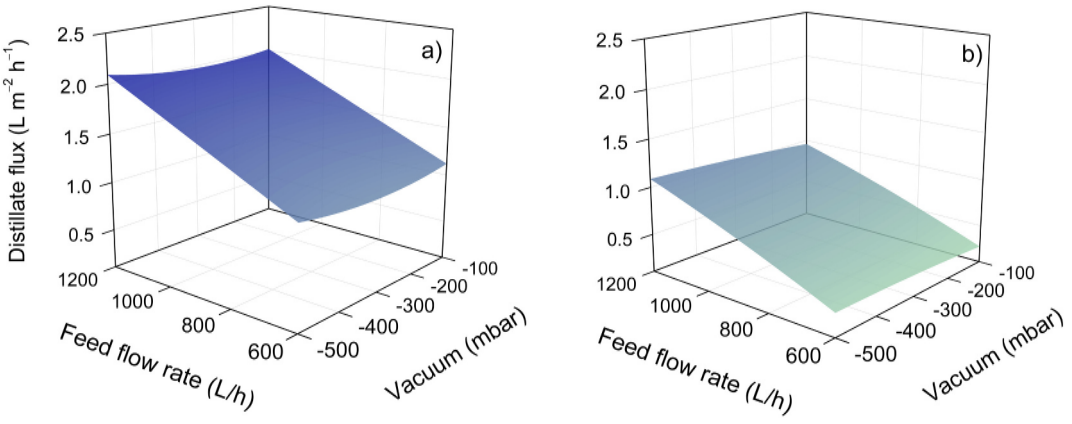

Fig. 3. Modeled distillate flux values are reported as a function of applied vacuum and feed flow rate. Figure a) refers to a feed solution with 5 g/L of NaCl while in b) the feed concentration is 150 g/L. The surfaces shade has visual purpose only, and it does not refer to a quantitative scale.

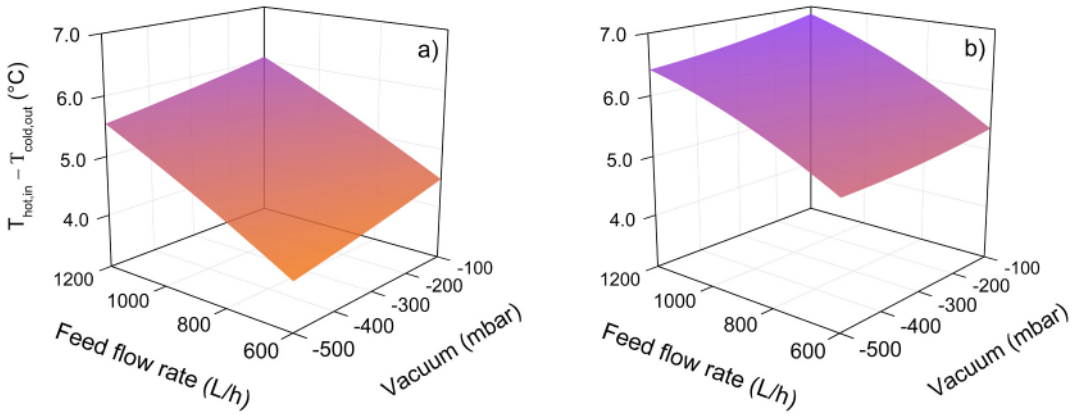

Fig. 4. Modeled temperature difference values between the feed hot inlet and the feed cold outlet are reported as a function of applied vacuum and feed flow rate. Figure a) refers to a feed solution with 5 g/L of NaCl while in b) the concentration is 150 g/L. The surfaces shade has visual purpose only, and it does not refer to a quantitative scale.

proportional to the amount of heat that the heat source needs to transfer to the feed stream to reach the target temperature. The obtained results are reported in Fig. 4.

Analogous trends of temperature difference were recorded for the two investigated feed salinities. The modeled surfaces highlight that an increase in feed flow rate always translated into an increase in temperature difference between the cold outlet and the hot inlet (and thus into a larger STEC), while an increase in applied vacuum led to a decrease in temperature difference and thus to a STEC reduction. It is important to point out that at high salinity values the effect of applied vacuum becomes small and thus the dominant regulating factor remains the feed flow rate. In general terms, as previously discussed by Hardikar et al. [37], in pilot-scale AGMD systems, the effective trans-membrane temperature difference, i.e. the driving force, is roughly one order of magnitude lower than the one of the set hot and cold inlet temperatures. Typical values of temperature difference are between 3 °C and 7 °C when condenser and evaporator inlets are set at 30 °C and 70 °C, respectively. This mechanism is the main reason for the relatively low distillate fluxes recorded in this research (see Fig. 2 and Fig. 3) and in most of the other pilot-scale studies, especially when compared to bench-scale results.

The trends of temperature difference may be rationalized considering the various heat flow mechanisms occurring across the membrane and within the channels. An increase in feed flow rate always produced an increase in the temperature difference between the two membrane sides leading consequently to a substantially higher distillate flux, i.e. productivity. This effect is largely caused by lowering the feed residence time in the flow channel, consequently reducing the heat transfer between the two membrane sides and thus diminishing the feed stream preheating [15]. The decrease in temperature difference when increasing vacuum values may be attributed to the enhanced latent heat flux sustaining the heat transfer between the condensing distillate and the cold feed side of the membrane, hence increasing the temperature of the latter.

The trends in distillate flux and temperature difference discussed above consequently affect the STEC reported in Fig. 5. First, note that the modeled STEC values differ considerably in Fig. 5a and Fig. 5b (the color scale is the same to highlight the absolute values difference while the z-axis is different to properly show the surfaces shapes). For the low-salinity case, a trade-off between productivity and STEC was observed when changing the feed flow rate: increasing this parameter was detrimental from the perspective of thermal energy consumption (Fig. 5a), even if it led to a distillate flux increase (Fig. 3a). However, according to Eq. (2), the higher achieved productivity was not sufficient to counteract the combined negative effects of higher temperature difference and higher feed flow rate itself on energy consumption, which was higher as a consequence. On the other hand, increasing the magnitude of the vacuum would produce small effects on productivity and a slight decrease in STEC.

Results relative to the hyper-saline scenario are reported in Fig. 5b. When considering the influence of feed flow rate, a non-monotonous trend was observed, with the STEC decreasing with feed flow rate and reaching a shallow minimum around 1000 L/h. To the best of our knowledge, a similar shape was previously recorded only in a research

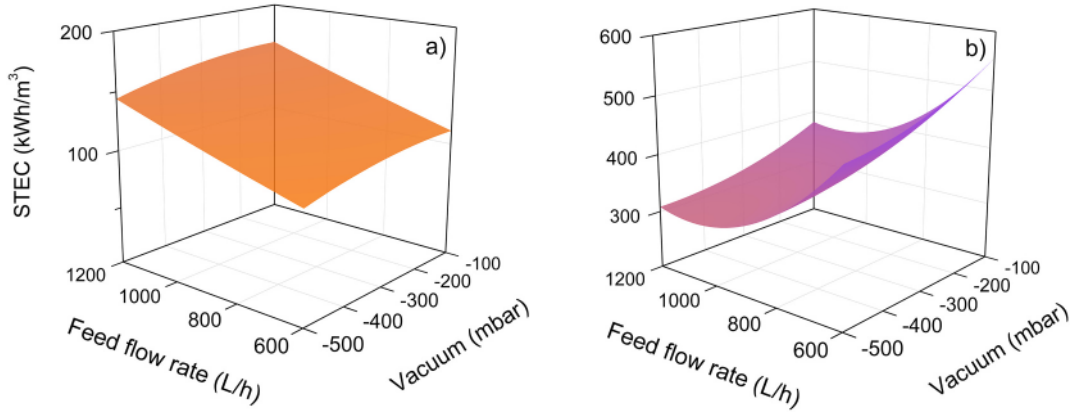

Fig. 5. Modeled specific thermal energy consumption values are reported as a function of applied vacuum and feed flow rate. Figure a) is referring to a feed solution with 5 g/L of NaCl while in b) the concentration was 150 g/L.

by Winter et al. [22], and modeled by Swaminathan et al. [13] and by Hardikar et al. [15]. This result implies that when using a hyper-saline stream, a system optimization is possible and that a best feed flow rate exists that would maximize the productivity while minimizing the specific thermal energy consumption of the process. In summary, as discussed by Hardikar et al. [15], the flow rate that minimizes the STEC is zero at zero salinity, and it increases as the salinity increases as showed in the results of Fig. 5.

To account for the overall energy consumption of the process also the SEEC necessary to circulate the water through the membrane channels was evaluated and the related results are reported in Table S2 in the Supporting Information. Note that the energy required to generate the vacuum and to cool down the system through the cooling loop should be addressed, since they typically play an important role in pilot-scale MD systems. Overall, the absolute values of the electrical energy consumption were orders of magnitude lower than the thermal energy necessary to heat up the feed stream. Recorded SEEC values increased as feed stream salinity increased since the latter was associated to a reduction of distillate production and an increase in the hydraulic pressure inside the membrane channels. Obtained SEEC results ranged approximately from 0.1 $kWh_{el}{\cdot}m^{-3}$ to 1 $kWh_{el}{\cdot}m^{-3}$, aligned with recent literature results obtained with the same system configuration [27,36]. However, for a more accurate analysis of the quality of the energy, other than quantity, and for a fairer comparison between electricity and low-grade heat requirements, a thorough exergetic analysis should be conducted. The latter, useful also to identify inefficiencies, is out of the scope of this work.

3.3. Quality of the product distillate water: vapor and pore flows

While it is established that distillate quality depends on the operating conditions, e.g., applied vacuum, feed flow rate, feed salinity, and operating temperatures, the prediction of AGMD systems selectivity is still challenging, especially in hyper-saline scenarios [14,19,25]. One parameter that could partly unravel the selectivity of the process is the salt flux. The salt flux results obtained in this study are reported in Fig.S3 in the Supporting Information. In summary, Fig.S3 suggests that an increase in feed flow rate or in applied vacuum always translates into a larger salt flux. This phenomenon may be rationalized by the increasing TMP which in turn is the parameter regulating the pore flow [14,25,31]. However, salt flux alone cannot fully explain the selectivity behavior of the process. It might not necessarily represent a reliable predictor of distillate quality, nor a stand-alone selectivity indicator, since salt flux is dependent on liquid distillate flux (see Eq. (5)), a correlation that was corroborated experimentally in this study. On the other hand, the salinity normalized salt flux may highlight the salt transport mechanisms across the membrane when it is plotted against the TMP (Fig.S4 in the Supporting Information). If pore flow occurs due to membrane 'defects', it is assumed to be a linear function of the TMP [31], whereas when pore flow is due to membrane wetting the liquid distillate flux should present an increasing gradient with respect to the TMP [38]. However, the data collected in this study and reported in Fig.S4 do not fully corroborate either of the two hypotheses and leave space for further investigations of the pore-flow phenomena.

To maintain generality and to provide a clear and straightforward selectivity analysis the salt rejection should be instead evaluated. The rejection results obtained in this study are reported in Fig. 6 where the LRV is plotted against the trans-membrane pressure. The rejection was high in all the tests and above 99.1 % (above 2-$\log_{10}$). Nevertheless, the data highlight that the rejection of the membrane was consistently lower when the feed stream contained high salt concentration, especially at low TMP values. This may be explained by the decrease in distillate flux when increasing the feed stream salinity that directly translates into a rejection decrease [7,14]. Moreover, the plot suggests that the rejection was largely regulated by the TMP. As reported in Table 3, the TMP is calculated as the sum of the applied vacuum and the average evaporator channel pressure along the module, the latter related to the feed flow rate. Note that the impact of applied vacuum on TMP was dominant in this study, although under different operating conditions the main contributor might be different and it should be addressed case by case. Pressure data related to the 150 g/L salinity are reported in Table S3 in the Supporting Information. Notice that the applied vacuum values slightly differ from the model set points because of the intrinsic precision of the relief valve, however the precision was always higher than 95 % and did not affect the obtained results.

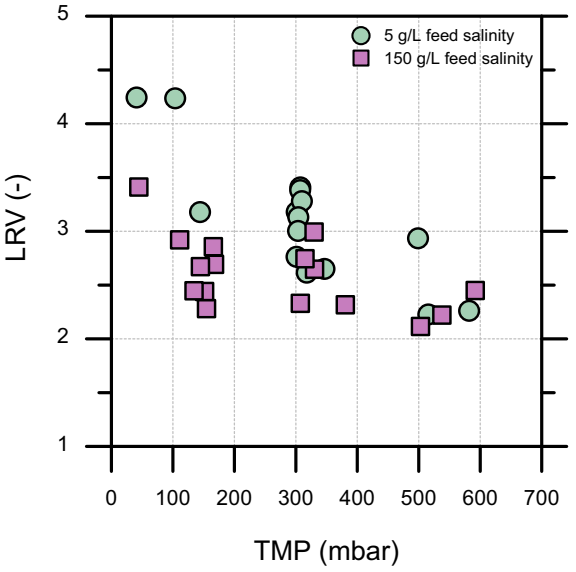

Fig. 6. To evaluate the selectivity of the process the LRV is reported as a function of the trans-membrane pressure difference calculated as the average pressure along the evaporator channel plus applied vacuum. Green circles refer to a feed stream concentration of 5 g/L of NaCl while pink squares refer to a feed stream concentration of 150 g/L of NaCl.

Table 3
Operating conditions and resulting trans-membrane pressure values when operating at 5 g/L feed salinity. The evaporator pressure column refers to the average hydraulic pressure along the evaporator channel.

Applied vacuum (mbar)	Feed flow rate ($L \cdot h^{-1}$)	Evaporator pressure (mbar)	TMP (mbar)
19	900	21	41
99	1,200	45	144
101	600	3	104
291	1,324	56	347
291	900	10	301
292	900	13	304
295	900	12	307
295	900	12	307
298	900	12	310
299	476	2	301
478	1,200	37	515
496	600	2	499
573	900	9	582

4. Conclusion

Vacuum-assisted air gap membrane distillation represents a promising technology for the concentration of hyper-saline streams achieving near zero liquid discharge. However, further implementation of this technical strategy can be limited because few studies dealing with the scalability and the behavior of pilot- and full-scale V-AGMD systems have been recently published. This research unraveled the effect of feed stream salinity and operating conditions (i.e. feed flow rate and applied

vacuum) on productivity, energy consumption, and selectivity of a pilot-scale V-AGMD system. In summary, the main findings of this study are: i) feed flow rate had a stronger impact on distillate flux than applied vacuum even if an increase in both led to higher productivity. ii) When a hyper-saline feed stream was used, the productivity decreased drastically compared to feed solutions characterized by low salinity. iii) The specific thermal energy consumption increased pseudo-linearly with feed flow rate at low salinity values while in an hyper-saline scenario when increasing the feed flow rate a decrease in STEC was observed (a minimum value of STEC can be identified). iv) an increase in vacuum led to a slight increase in distillate flux and thus to a more effective pre-heating phase that, combined, translated into a system energy performance improvement. Regarding the process selectivity, data suggest that the salt rejection was regulated by the trans-membrane pressure: an increase in pressure difference translated into a decrease in rejection. The results also indicated that, while increasing the feed flow rate led to an improvement in productivity, it also led to an increase in salt flux. Additionally, vacuum regulated the trans-membrane pressure and thus its increase lowered the salt rejection.

Nomenclature

Acronyms

AGMD	Air gap membrane distillation
ANOVA	Analysis of variance
CCD	Central composite design
LEP	Liquid entry pressure
MD	Membrane distillation
PLC	Programmable logic controller
RSM	Response surface methodology
TMP	Trans-membrane pressure
V-AGMD	Vacuum-assisted air gap membrane distillation
ZLD	Zero liquid discharge

Symbols

ΔP_{drop}	*bar*, hydraulic pressure drop over the membrane module
η	$-$, efficiency of the water circulating pump
ρ_f	$kg{\cdot}m^{-3}$, feed density
A	m^2, membrane active area
C	$J{\cdot}kg^{-1}{\cdot}K^{-1}$, specific heat capacity
c_d	$g{\cdot}L^{-1}$, concentration of NaCl in the produced distillate
c_f	$g{\cdot}L^{-1}$, concentration of NaCl in the feed stream
J_s	$g{\cdot}m^{-2}{\cdot}h^{-1}$, salt flux
J_w	$L{\cdot}m^{-2}{\cdot}h^{-1}$, total water flux
$J_{w,l}$	$L{\cdot}m^{-2}{\cdot}h^{-1}$, liquid water flux
$J_{w,v}$	$L{\cdot}m^{-2}{\cdot}h^{-1}$, vapor water flux
Q_f	$L{\cdot}h^{-1}$, feed flow rate
$T_{cold,in}$	$^{\circ}C$, cold inlet temperature
$T_{cold,out}$	$^{\circ}C$, cold outlet temperature
$T_{hot,in}$	$^{\circ}C$, hot inlet temperature
$T_{hot,out}$	$^{\circ}C$, hot outlet temperature
V_d	L, volume of distillate collected in the time frame Δt
LRV	$-$, log removal value
R	%, salt rejection
SEEC	$kWh_{el}{\cdot}m^{-3}$, specific electrical energy consumption
STEC	$kWh_{th}{\cdot}m^{-3}$, specific thermal energy consumption

CRediT authorship contribution statement

Marco Malaguti: Writing – original draft, Investigation, Formal analysis, Data curation, Conceptualization. **Luke K. Presson:** Writing – review & editing, Methodology, Investigation, Formal analysis. **Alberto Tiraferri:** Writing – review & editing, Visualization, Supervision, Funding acquisition. **Kerri L. Hickenbottom:** Writing – review & editing, Supervision, Resources, Project administration, Funding acquisition. **Andrea Achilli:** Writing – review & editing, Supervision, Resources, Project administration, Funding acquisition.

Declaration of competing interest

The Authors declare no Competing Financial or Non-Financial Interests.

Data availability

Data will be made available on request.

Acknowledgments

This research was funded by the Environmental Security Technology Certification Program (ESTCP) Award ER19-5242. We thank Pete Shickel from Porometer (Aptco Technologies NV, Nazareth, Belgium) for testing our membrane for pore size distribution.

Appendix A. Supplementary data

Supplementary data to this article can be found online at https://doi.org/10.1016/j.desal.2024.117511.

References

[1] L.K. Presson, V. Felix, M. Hardikar, A. Achilli, K.L. Hickenbottom, Fouling characterization and treatment of water reuse concentrate with membrane distillation: do organics really matter, Desalination 553 (2023) 116443.
[2] T. Tong, M. Elimelech, The global rise of zero liquid discharge for wastewater management: drivers, technologies, and future directions, Environ. Sci. Technol. 50 (13) (2016) 6846–6855.
[3] C.A. Quist-Jensen, F. Macedonio, E. Drioli, Membrane technology for water production in agriculture: desalination and wastewater reuse, Desalination 364 (2015) 17–32.
[4] M. Morciano, M. Malaguti, F. Ricceri, A. Tiraferri, M. Fasano, Process optimization of osmotic membrane distillation for the extraction of valuable resources from water streams, npj Clean Water 7 (1) (2024) 1.
[5] V. Yangali-Quintanilla, Z. Li, R. Valladares, Q. Li, G. Amy, Indirect desalination of red sea water with forward osmosis and low pressure reverse osmosis for water reuse, Desalination 280 (1) (2011) 160–166.
[6] M. Malaguti, L. Craveri, F. Ricceri, V. Riggio, M. Zanetti, A. Tiraferri, Dewatering of scenedesmus obliquus cultivation substrate with microfiltration: potential and challenges for water reuse and effective harvesting, Engineering.
[7] R. Schwantes, L. Bauer, K. Chavan, D. Dücker, C. Felsmann, J. Pfafferott, Air gap membrane distillation for hypersaline brine concentration: operational analysis of a full-scale module–new strategies for wetting mitigation, Desalination 444 (2018) 13–25.
[8] M. Bindels, J. Carvalho, C.B. Gonzalez, N. Brand, B. Nelemans, Techno-economic assessment of seawater reverse osmosis (swro) brine treatment with air gap membrane distillation (agmd), Desalination 489 (2020) 114532.
[9] A.L. McGaughey, A.E. Childress, Wetting indicators, modes, and trade-offs in membrane distillation, J. Membr. Sci. 642 (2022) 119947.
[10] H.C. Duong, A.R. Chivas, B. Nelemans, M. Duke, S. Gray, T.Y. Cath, L.D. Nghiem, Treatment of ro brine from csg produced water by spiral-wound air gap membrane distillation — a pilot study, Desalination 366 (2015) 121–129.
[11] M.R. Qtaishat, F. Banat, Desalination by solar powered membrane distillation systems, Desalination 308 (2013) 186–197.
[12] M. Inkawhich, J. Shingler, R.S. Ketchum, W. Pan, R.A. Norwood, K. L. Hickenbottom, Temporal performance indicators for an integrated pilot-scale membrane distillation-concentrated solar power/photovoltaic system, Appl. Energy 349 (2023) 121675.
[13] J. Swaminathan, H.W. Chung, D.M. Warsinger, J.H. Lienhard V, Energy efficiency of membrane distillation up to high salinity: evaluating critical system size and optimal membrane thickness, Appl. Energy 211 (2018) 715–734.
[14] A. Ruiz-Aguirre, J. A. Andrés-Mañas, G. Zaragoza, Evaluation of permeate quality in pilot scale membrane distillation systems, Membranes 9 (6).
[15] M. Hardikar, I. Marquez, T. Phakdon, A.E. Sáez, A. Achilli, Scale-up of membrane distillation systems using bench-scale data, Desalination 530 (2022) 115654.
[16] A. Tiraferri, M. Malaguti, M. Mohamed, M. Giagnorio, F.J. Aschmoneit, Standardizing practices and flux predictions in membrane science via simplified equations and membrane characterization, npj Clean Water 6 (1) (2023) 58.

[17] E. Guillén-Burrieza, G. Zaragoza, S. Miralles-Cuevas, J. Blanco, Experimental evaluation of two pilot-scale membrane distillation modules used for solar desalination, J. Membr. Sci. 409-410 (2012) 264–275.
[18] A. Ruiz-Aguirre, J.A. Andrés-Mañas, J.M. Fernández-Sevilla, G. Zaragoza, Experimental characterization and optimization of multi-channel spiral wound air gap membrane distillation modules for seawater desalination, Sep. Purif. Technol. 205 (2018) 212–222.
[19] J.A. Andrés-Mañas, I. Requena, G. Zaragoza, Characterization of the use of vacuum enhancement in commercial pilot-scale air gap membrane distillation modules with different designs, Desalination 528 (2022) 115490.
[20] L. Francis, F. E. Ahmed, N. Hilal, Advances in membrane distillation module configurations, Membranes 12 (1).
[21] G. Rao, S.R. Hiibel, A. Achilli, A.E. Childress, Factors contributing to flux improvement in vacuum-enhanced direct contact membrane distillation, Desalination 367 (2015) 197–205.
[22] D. Winter, J. Koschikowski, M. Wieghaus, Desalination using membrane distillation: experimental studies on full scale spiral wound modules, J. Membr. Sci. 375 (1) (2011) 104–112.
[23] J. Swaminathan, H.W. Chung, D.M. Warsinger, J.H. Lienhard V, Membrane distillation model based on heat exchanger theory and configuration comparison, Appl. Energy 184 (2016) 491–505.
[24] D. Woldemariam, A. Martin, M. Santarelli, Exergy analysis of air-gap membrane distillation systems for water purification applications, Appl. Sci. 7 (3).
[25] J.A. Andrés-Mañas, A. Ruiz-Aguirre, F.G. Acién, G. Zaragoza, Performance increase of membrane distillation pilot scale modules operating in vacuum-enhanced air-gap configuration, Desalination 475 (2020) 114202.
[26] R.d.S. Silva, H. Ramlow, B.d.C. Santos, H.B. Madalosso, R.A.F. Machado, C. Marangoni, Membrane distillation: experimental evaluation of liquid entry pressure in commercial membranes with textile dye solutions, J. Water Process. Eng. 44 (2021) 102339.
[27] J.A. Andrés-Mañas, I. Requena, G. Zaragoza, Membrane distillation of high salinity feeds: steady-state modelling and optimization of a pilot-scale module in vacuum-assisted air gap operation, Desalination 553 (2023) 116449.
[28] A. Boubakri, A. Hafiane, S.A.T. Bouguecha, Application of response surface methodology for modeling and optimization of membrane distillation desalination process, J. Ind. Eng. Chem. 20 (5) (2014) 3163–3169.
[29] P. Gharbani, A. Mehrizad, S.A. Mosavi, Optimization, kinetics and thermodynamics studies for photocatalytic degradation of methylene blue using cadmium selenide nanoparticles, npj Clean Water 5 (1) (2022) 34.
[30] A. Tiraferri, N.Y. Yip, A.P. Straub, S. Romero-Vargas Castrillon, M. Elimelech, A method for the simultaneous determination of transport and structural parameters of forward osmosis membranes, J. Membr. Sci. 444 (2013) 523–538.
[31] M. Hardikar, V. Felix, L.K. Presson, A.B. Rabe, L.A. Ikner, K.L. Hickenbottom, A. Achilli, Pore flow and solute rejection in pilot-scale air-gap membrane distillation, J. Membr. Sci. 676 (2023) 121544.
[32] M. Rezaei, D.M. Warsinger, J.H. Lienhard V, M.C. Duke, T. Matsuura, W. M. Samhaber, Wetting phenomena in membrane distillation: mechanisms, reversal, and prevention, Water Res. 139 (2018) 329–352.
[33] L. Chen, P. Xu, H. Wang, Interplay of the factors affecting water flux and salt rejection in membrane distillation: a state-of-the-art critical review, Water 12 (10).
[34] L. Eykens, I. Hitsov, K. De Sitter, C. Dotremont, L. Pinoy, B. Van der Bruggen, Direct contact and air gap membrane distillation: differences and similarities between lab and pilot scale, Desalination 422 (2017) 91–100.
[35] Z. Liu, Q. Gao, X. Lu, Z. Ma, H. Zhang, C. Wu, Experimental study of the optimal vacuum pressure in vacuum assisted air gap membrane distillation process, Desalination 414 (2017) 63–72.
[36] H.C. Duong, P. Cooper, B. Nelemans, T.Y. Cath, L.D. Nghiem, Evaluating energy consumption of air gap membrane distillation for seawater desalination at pilot scale level, Sep. Purif. Technol. 166 (2016) 55–62.
[37] M. Hardikar, I. Marquez, A. Achilli, Emerging investigator series: membrane distillation and high salinity: analysis and implications, Environ. Sci. Water Res. Technol. 6 (6) (2020) 1538–1552.
[38] K.W. Lawson, D.R. Lloyd, Membrane distillation, J. Membr. Sci. 124 (1) (1997) 1–25.